Surface Topography: Metrology and Properties

PAPER

Quantitative calibration of conductive pattern growth via electroless copper plating at nano-resolution

To cite this article: Yanqiu Chen *et al* 2020 *Surf. Topogr.: Metrol. Prop.* **8** 035003

View the article online for updates and enhancements.

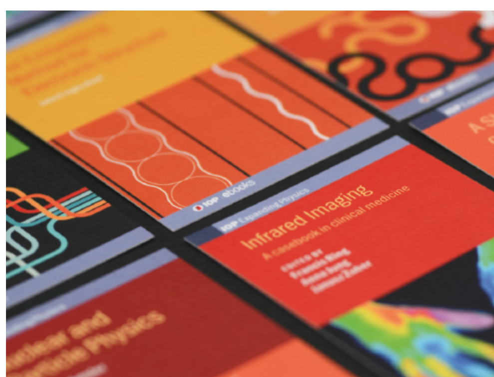

IOP ebooks™

Bringing together innovative digital publishing with leading authors from the global scientific community.

Start exploring the collection–download the first chapter of every title for free.

This content was downloaded from IP address 129.100.83.74 on 15/07/2020 at 04:51

Surface Topography: Metrology and Properties

RECEIVED
27 May 2020

REVISED
22 June 2020

ACCEPTED FOR PUBLICATION
6 July 2020

PUBLISHED
14 July 2020

PAPER

Quantitative calibration of conductive pattern growth via electroless copper plating at nano-resolution

Yanqiu Chen[1,2,6], Yu Liu[1,2,6,7], Wei Xu[1], Yang Zhang[3] and Heng-Yong Nie[4,5,7]

1 School of Mechanical Engineering, Jiangnan University, 214122 Wuxi, People's Republic of China
2 Jiangsu Key Lab of Advanced Food Manufacturing Equipment and Technology, Jiangnan University, 214122 Wuxi, People's Republic of China
3 Department of Mechanical Engineering, Technical University of Denmark, 2800 Kgs. Lyngby, Denmark
4 Surface Science Western, The University of Western Ontario, 999 Collip Circle, London, N6G 0J3 Ontario, Canada
5 Department of Physics and Astronomy, The University of Western Ontario, London, N6A 3K7 Ontario, Canada
6 These authors contribute equally to this work.
7 Authors to whom any correspondence should be addressed.

E-mail: yuliu@jiangnan.edu.cn and hnie@uwo.ca

Keywords: flexible conductive patterns, electroless plating, nanoscale characterization, ToF-SIMS, AFM

Abstract

In compositions of flexible electronics, conductive strands with high flexibility are crucial. Today, electroless plating for metallization of plastic substrates is favourable, due to its low cost, broad material compatibility, high conductivity, and potential for batch process. It is important to investigate the surface chemistry during electroless plating for better quantization of conductive patterns during the growth with nanoscopic resolution. Wherein, time-of-flight secondary ion mass spectrometry (TOF-SIMS) and atomic force microscopy (AFM) are combinatively used to follow surface chemistry of electroless-plated copper layers on a silver-activated polyimide film, in a bath containing mainly a copper source, two chelates and a reducing agent of formaldehyde. TOF-SIMS results show that surface contaminants detected on the copper layers can be traced back to the chemicals used in the plating bath, some of which impact copper purity. Shallow depth profiling of a copper layer reveals the variations of copper oxide and surface contaminants. AFM results innovate the instrumentations for probing surface morphologies in relationship to the electroless plating process as well. The results demonstrated a powerful technique in understanding the surface chemistry of electroless-plated copper layers on an activated insulating substrate and playing a calibration role in next step for industrialization.

1. Introduction

Flexible electronics on plastic substrates have attracted significant interest from the research communities in energy harvesting, displays, smart packaging, wearable electronics, and bio-integrated sensors and actuators [1–5]. In compositions of flexible electronics, conductive strands with high flexibility are crucial as interconnections [6], antennas [7], and more complex functional patterns [8–10]. The effective deposition methods of flexible conductive patterns on plastics are therefore in high demand for layered manufacturing of various flexible electronics, in which the digital inkjet printing method is of paramount importance in allowing accurate deposition and minimum waste generation, conformable patterning, and high mechatronic tunability [11]. Although many practices with digital inkjet printing have been reported for direct deposition of metal nanoparticle (NP) [12, 13], a substantial amount of surfactants, as required for NP dispersion, need to be effectively removed [14–16] by high temperature sintering [17–19]. This posttreatment not only burdens the energy consumption but also limits the broader selection of substrate materials.

Lately, electroless copper plating for metallization of plastics and textiles has been widely studied as an essential metallization approach for flexible electronics [20–23], which is a highly complicated redox process of converting copper salt to metallic copper [24–26]. For further improving the cost-effectiveness and printability, silver ion-based ink as the activating agent was developed for copper electroless

© 2020 IOP Publishing Ltd

metallization [27, 28]. Wherein, an insulating substrate needs to be catalytically activated for allowing copper deposition to take place on top of the substrate, such as by immersing the substrate in a silver nitrate solution [25, 26]. Because some substrates, e.g. polyimides (PIs), are rather inert, or hydrophobic, a basic solution treatment is usually used to render their surface hydrophilic [29]. The electroless copper plating mechanisms [24, 25], especially the requirement of dual chelating agents and other additives [30] and control of the plating rates and quality of plated metal films [26], as well as impact of surface treatment of substrate film on adhesion enhancement of the electroless copper deposits [31], have been explored. Growth stability, rates, surface morphology and conductivity associated with electroless copper depositions have also been extensively investigated [32–34].

The quality of an electroless plated metal on a polymer substrate relies on sensitization and activation of the substrate. There have been studies concentrated on the sensitization and activation of various substrates including PI [29], polyethylene terephthalate [35], polycarbonate and other polymers [36], as well as silica [37]. Surface chemistry of the plated metal layer has been analyzed using XPS [29, 35, 37], which differentiates the metallic state from the ionic state. However, to our knowledge, there has been no report concentrating on surface contamination of the three surfaces in the electroless copper plating, namely, the sensitized PI surface upon a necessary solution treatment, the activated surface subsequently obtained by immersing the PI film in a silver nitrate solution and the final copper deposit. Presented in this study is a time-of-flight secondary ion mass spectrometry (TOF-SIMS) [38] investigation to fully understand the surface chemistry in each step of the electroless copper plating process. TOF-SIMS is a surface-sensitive technique probing the outermost 1–3 nm of the surface via detection of (secondary) ions generated by bombarding a primary ion beam (e.g., Bi_3^+) onto the sample surface. Surface chemistry is explored via the detection of these secondary ions, which contains elements, functional groups, molecular fragments, and even molecular ions. Therefore, TOF-SIMS provides superior chemical selectivity for exploring surface chemistry [38–43]. With a sputter ion beam to remove substances from the surface, TOF-SIMS is capable of depth profiling [44–46] variations of compositions at a depth resolution better than 1 nm. This is especially powerful in probing, e.g., the thickness of 'native' oxide of metals [47].

2. Experimental methods

In accordance with our previous work [33], all treatments associated with copper plating on PI films (Kapton 100HN) were done in aqueous solutions. The PI film was ultrasonicated in ethanol for 5 min, followed by being immersed in an 80 g l^{-1} sodium hydroxide (NaOH) solution for 10 min for opening the imide rings, resulting in the hydrophilicity of the PI film. This served to promote the catalytical activation of the PI film upon its immersion in a 17 g l^{-1} silver nitrate ($AgNO_3$) solution for a short and long period of 1 and 20 min, respectively. The activated PI films were directly taken out from the silver nitrate solution and dried. These naturally dried PI films were used for surface analysis. The activated PI films subjected to the $AgNO_3$ solution for 1 min were used for subsequent electroless copper plating experiment via immersion in the electroless copper plating solution for 0.5, 3 and 10 min. The electroless plating bath was a mixture of the chemicals shown in table 1.

In the electroless copper plating bath, copper ions, Cu^{2+}, from the cupric sulfate were reduced by formaldehyde in a basic solution controlled by sodium hydroxide. Two chelating agents, disodium ethylenediaminetetraacetate (Na_2-EDTA) and potassium sodium tartrate tetrahydrate, were used to ensure the reduction of Cu^{2+} and deposition of metallic copper at the activated PI film surface. In this electroless plating approach, silver ions from the pre-deposited silver nitrate were also reduced, which catalyzed the initial formation of metallic copper on the surface. Samples of the copper layer plated on a PI film were briefly washed with de-ionized water.

A TOF-SIMS instrument, model TOF-SIMS IV from ION-TOF GmbH (Germany) was used to follow the surface chemistry of the $AgNO_3$-activated surface and the electroless plated copper film. The instrument was operated by bombarding the sample surface using a pulsed (~1 ns) 25 keV Bi_3^+ primary ion beam (target current ~1 pA) to generate secondary ions, which were extracted by an electric field, and their times of flight through a reflectron type of tube were measured. A low energy electron beam was then flooded over the sample for charge compensation, which completed the 100-μs cycle of one shot of the primary ion. The base pressure of the analysis chamber of the instrument was on the order of 10^{-7} mbar. The measured flight time scale was calibrated to mass/charge (m/z) ratio via known species such as hydrogen, carbon and hydrocarbons. The secondary ion mass spectra were collected for 50 scans, each at 128 × 128 pixels, with one shot of pulsed primary ion beam per pixel, over an area of 500 μm × 500 μm. The mass resolution for CH^-, C_2H^-, CNO^- $C_2H_3^+$, $C_4H_7^+$ and Na_2OH^+ was 3100, 3900, 4100, 5000, 5300 and 7000, respectively. In order to depth profile the 10-min electroless plated copper layer, a 3 keV Cs^+ beam was used to sputter the surface in an area of 200 μm × 200 μm, within which negative ion mass spectra were collected over a smaller area (128 μm × 128 μm) within the sputter. The depth profile data were obtained by repeating the following cycle of sputtering the surface with the Cs^+ beam for 1 s followed by a 0.5-s pause before Bi_3^+ was used to analyse the newly generated surface.

The dynamic force mode of atomic force microscopy (AFM), a Park Systems XE-100 AFM (South Korea) was used to image the surface morphology of silver nitrate activated and copper plated PI films. AFM images consisting of 256 lines with each line having 256 data points were collected using cantilevers having a nominal spring constant of ~40 N m^{-1} and a resonance frequency of ~300 kHz (MikroMasch NSC15). The AFM images were collected in ambient air at room temperature.

3. Results and discussion

Shown in figure 1 are positive secondary ion mass spectra (in the m/z range of 20–150) for PI films treated by a NaOH solution (control) and subsequently immersed in an $AgNO_3$ solution for 1 and 20 min. The spectrum of the control is dominated by Na^+ and the second most abundant ion is Na_2OH^+. Other ions detected are hydrocarbons (e.g., $C_2H^+_{3,5}$, $C_3H^+_{3,5,7}$ and $C_4H^+_{7,9}$) having much less abundance. For a brief immersion of 1 min in the $AgNO_3$ solution, the most abundant ions are the two isotopes of silver, $^{107}Ag^+$ and $^{109}Ag^+$. This shows that the surface of the NaOH-treated PI film immersed in the $AgNO_3$ solution for 1 min renders a coverage of silver. The Na^+ level, though still strong, is much less than that of the control. Other major peaks are the ions of hydrocarbons. Also detected is a relatively weak silicone ion, $SiC_3H_9^+$, which is believed to be due to cross contamination as a silicone used in 3D printing of silicone elastomers is routinely dealt with in the lab. With elevated immersion time of 20 min, the Na^+ signals become minimal, suggesting that the residual sodium on the control was removed from the surface. The TOF-SIMS results shown in figure 1 confirmed that even an immersion time of 1 min is enough to deposit silver on the NaOH-treated PI film. Because TOF-SIMS probes the outermost 1–3 nm of the surface, the spectra for the 1- and 20-min treated samples show similar results.

Shown in figure 2 are spectra in m/z 150–335, from which four groups of peaks are observed on the $AgNO_3$-treated samples, while there are no abundant peaks observed on the control. The first one contains peaks from m/z 214 to 219, whose pattern resembles the combination of Ag_2^+ and Ag_2H^+ with their intensity ratio being ~1, as determined using the isotope cluster calculator of the TOF-SIMS software. The second one contains peaks at m/z 231, 233 and 235, which is simply Ag_2OH^+. The third one, comprised of peaks from m/z 239 to 244, resembles the pattern of $Ag_2C_2H^+$ and Ag_2CN^+ at an intensity ratio ~0.9. The last one is the silver cluster ion Ag_3^+.

The negative secondary ion mass spectra in the m/z range of 11–80 are shown in figure 3. The control shows characteristic ions to PI, that are CN^-, CNO^- and C_3N^-, as well as hydrocarbons (e.g., C_2H^-, C_4H^- and C_6H^-). Upon the $AgNO_3$ treatment, no matter whether the NaOH-treated PI film was immersed in $AgNO_3$ for 1 or 20 min, their TOF-SIMS results revealed that the surface shows the same chemistry that is dominated by NO_3^-. Also detected is NO_2^-, a fragment of nitrate. Nevertheless, the nitrogen-containing species are still strong on the $AgNO_3$-treated samples, suggesting that these PI substrate related species were present on the treated surface. This is believed to be due to adsorption of species dissolved from PI in the solution.

The spectra in figure 4 show that there are three silver-related species detected on the $AgNO_3$-treated samples, which are $Ag(CN)_2^-$ [i.e., $^{107}Ag(CN)_2^-$ and $^{109}Ag(CN)_2^-$], $Ag(NO_3)(CN)^-$ and $Ag(NO_3)_2(CN)^-$. The detection of $Ag(CN)_2^-$ indicates presence of silver cyanide (AgCN), which yields the negative ion species $Ag(CN)_2^-$. One the other hand, due to the abundant Ag^+ (figure 1) and CN^- (figure 2) generated from the ion bombardment, it is also possible that these two species combine in the space [48, 49] above the sample surface to form $Ag(CN)_2^-$. It is highly likely that $Ag(NO_3)(CN)^-$ forms in the space as a result of the combined Ag^+, NO_3^- and CN^- because they are hardly a structural entity existing on the $AgNO_3$-activated PI film surface. On the other hand, $Ag(NO_3)_2^-$ is mainly due to the presence of $AgNO_3$, which captures a NO_3^- ion and becomes the negative ion.

Shown in figure 5 are topographic images obtained by AFM on the control (the NaOH-treated PI film) and the PI films activated in an $AgNO_3$ solution for 1 and 20 min. The control shown in figure 5(a) is characterized by fiber-like structures, having a root mean square (RMS) roughness Rq of 11 nm. By contrast, as shown in figure 5(b), upon 1-min $AgNO_3$ treatment, the fiber-like structure disappeared. The surface became smoother, with its Rq being only 6 nm. This AFM result, coupled with the TOF-SIMS results shown in figure 1, indicate that the surface is covered

Table 1. Chemicals and their concentrations in the electroless plating bath.

Chemicals in plating bath	Concentration (g l^{-1})
Copper sulfate pentahydrate ($CuSO_4•5H_2O$)	12
Formaldehyde (HCHO)	15
Disodium ethylenediaminetetraacetate ($C_{10}H_{14}N_2Na_2O_8$)	21
Potassium sodium tartrate tetrahydrate ($KNaC_4H_4O_6•4H_2O$)	16
Sodium hydroxide (NaOH)	15

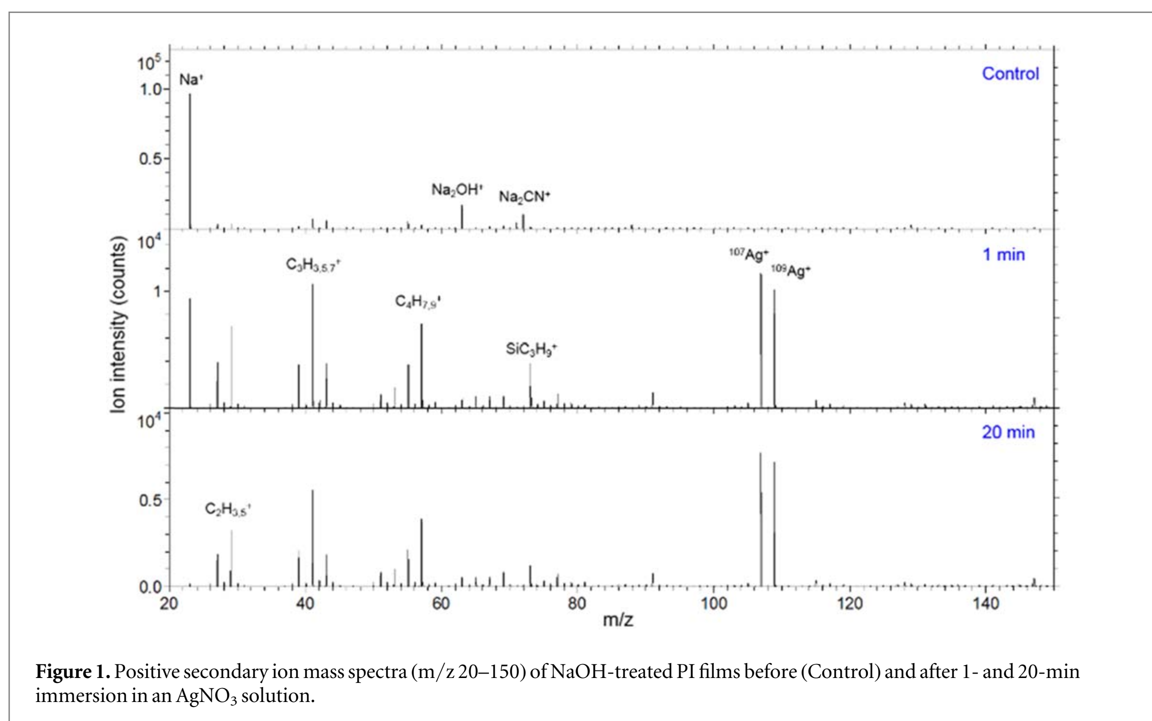

Figure 1. Positive secondary ion mass spectra (m/z 20–150) of NaOH-treated PI films before (Control) and after 1- and 20-min immersion in an $AgNO_3$ solution.

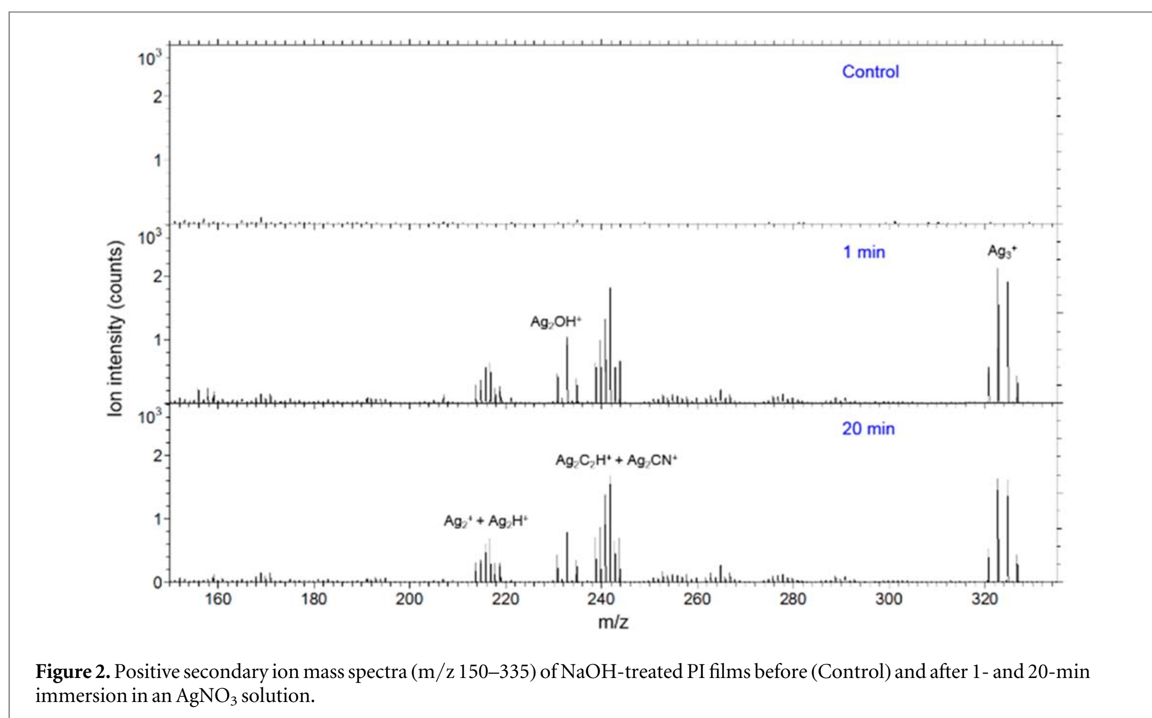

Figure 2. Positive secondary ion mass spectra (m/z 150–335) of NaOH-treated PI films before (Control) and after 1- and 20-min immersion in an $AgNO_3$ solution.

by a rather smooth layer containing silver upon even 1-min immersion in the $AgNO_3$ solution. The several aggregates observed in figure 5(b) might be due to residual $AgNO_3$ because the sample was taken out directly from the solution without washing. Another possibility is that they are silver-related aggregates formed with the sensitized PI. Due to the lack of presence of reducing agent in the $AgNO_3$ solution, the observed aggregates are likely a silver salt, rather than metallic silver, for which the detection of $Ag(CN)_2^-$ shown in figure 3 for the 1-min $AgNO_3$-treated sample can serve as a side evidence.

Figures 5(c) and (d) show the topographic images collected over two areas on the sample immersed in the solution for 20 min. The Rq for the images in figures 5(c) and (d) is 16 and 13 nm, respectively. This significant increase in roughness is due to the aggregates seen in figure 5(c) and needle-like features in figure 5(d). The aggregates in figure 5(c) appear to grow from those in figure 5(b) due to the prolonged immersion time. The needle-like features in figure 5(d) are believed to be crystals of the $AgNO_3$. It is thus apparent that longer immersion times resulted in a rougher surface, which is likely to impact the quality of the subsequent electroless-plated copper layer.

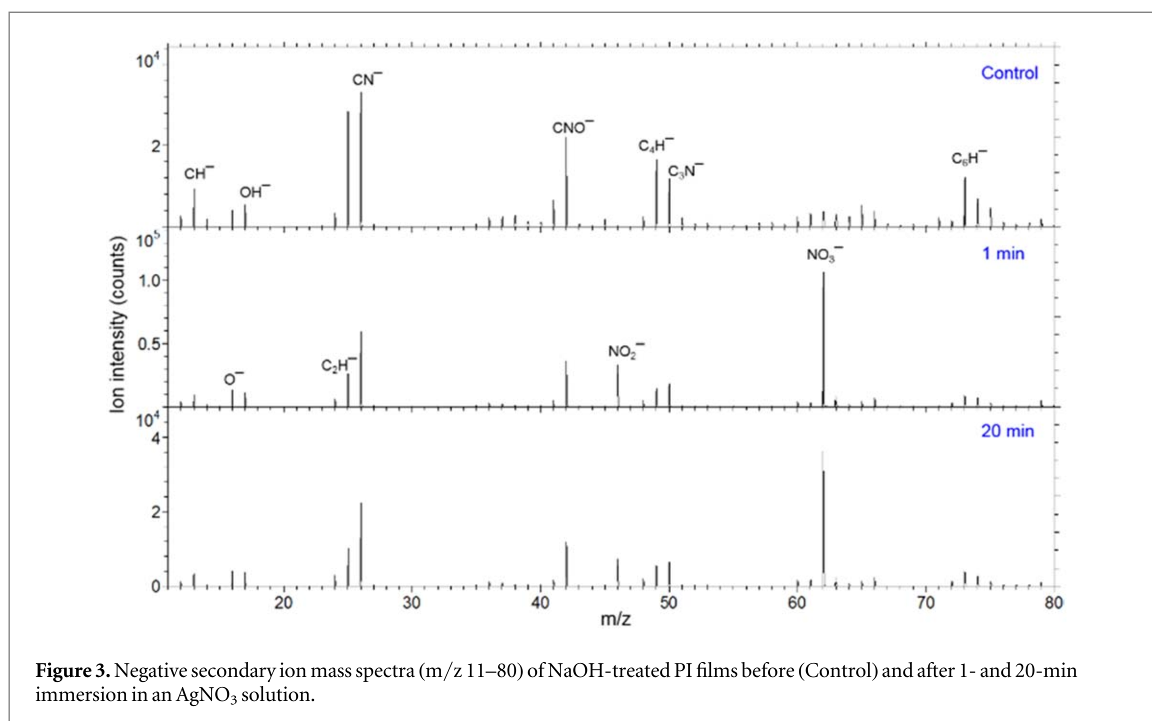

Figure 3. Negative secondary ion mass spectra (m/z 11–80) of NaOH-treated PI films before (Control) and after 1- and 20-min immersion in an $AgNO_3$ solution.

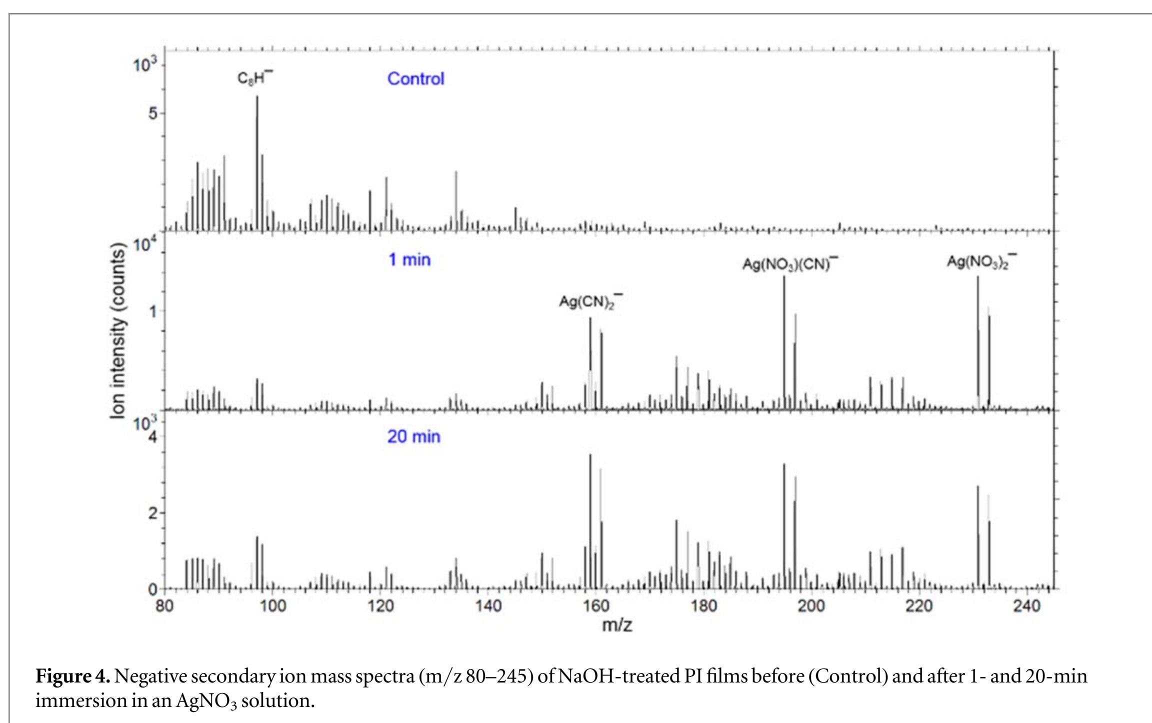

Figure 4. Negative secondary ion mass spectra (m/z 80–245) of NaOH-treated PI films before (Control) and after 1- and 20-min immersion in an $AgNO_3$ solution.

In addition, other factors impacting the quality of the subsequently electroless plated metal film include surface energy and seeding of silver, as well as solution state. The TOF-SIMS and AFM results confirmed that silver is deposited on the NaOH-treated PI film upon immersion in the $AgNO_3$ solution for only 1 min. There is thus no need to immerse the film in $AgNO_3$ for an elevated period for the purpose of activating the insulating PI surface for subsequent electroless copper plating.

The surface of copper films electroless-plated on the $AgNO_3$-activated PI film (for 1 min) as a function of plating time of 0.5, 3 and 10 min was analyzed using TOF-SIMS. Shown in figure 6 are positive secondary ion mass spectra in the range of m/z 20–170. The four most abundant ions are Na^+, K^+, Na_2OH^+ and $Na_2SO_3H_3^+$. As shown in figure 7, the ion intensity scales are adjusted to show other less abundant ions. Rather than the hydrocarbon ions mainly shown for the 0.5-min plated sample, the other ions are related to either sodium or potassium, such as Na_2^+, Na_2H^+, Na_2O^+, Na_2CN^+, $NaKOH^+$, Na_3O^+, $NaKSO_3H_3^+$ and $Na_3SO_4^+$. It thus becomes clear that the brief rinse of the sample following the electroless copper plating did

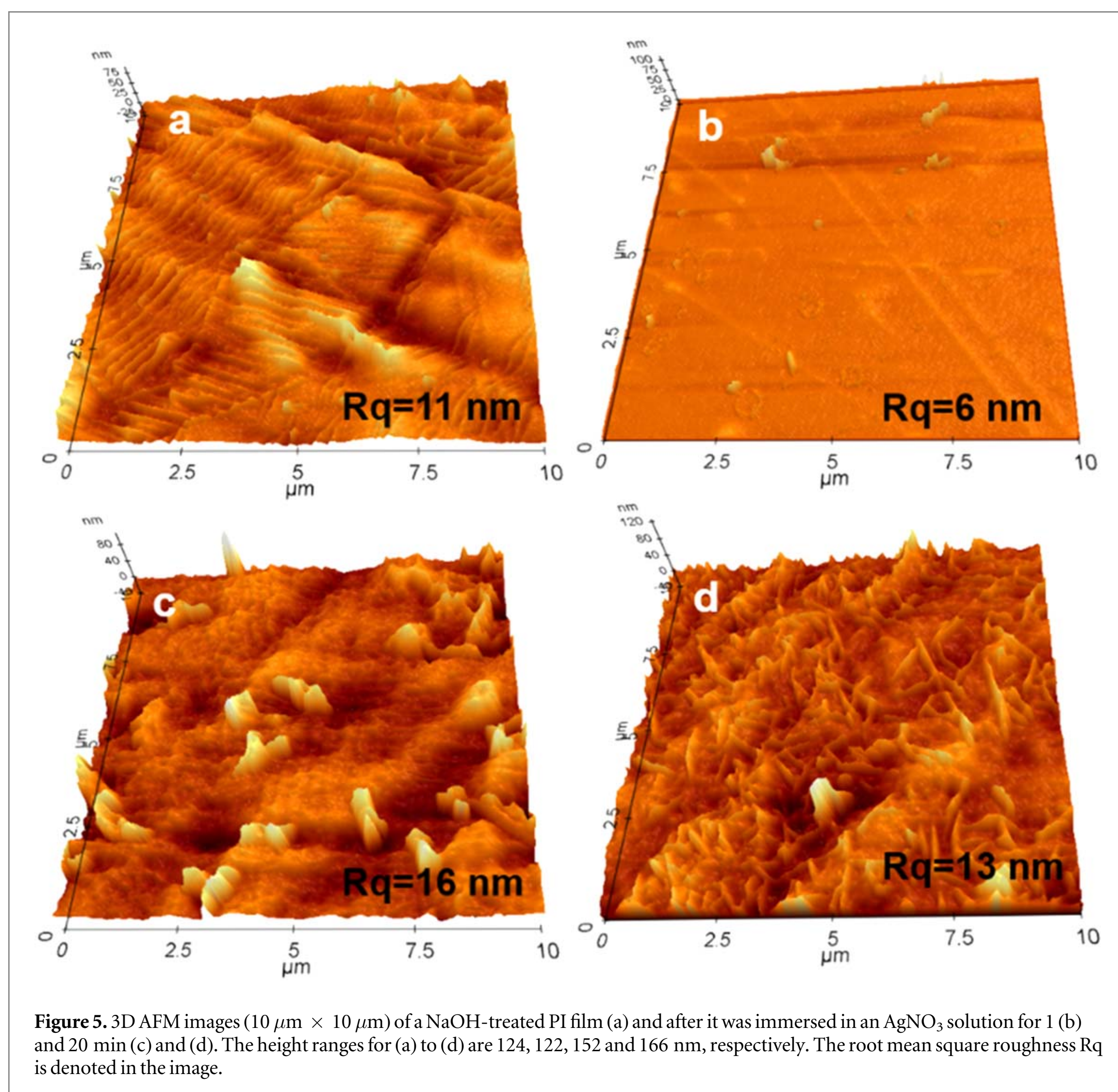

Figure 5. 3D AFM images (10 μm × 10 μm) of a NaOH-treated PI film (a) and after it was immersed in an $AgNO_3$ solution for 1 (b) and 20 min (c) and (d). The height ranges for (a) to (d) are 124, 122, 152 and 166 nm, respectively. The root mean square roughness Rq is denoted in the image.

not completely remove the sodium and potassium related species, which originate from NaOH and $KNaC_4H_4O_6•4H_2O$ in the plating bath. On the other hand, the detected ions that contain sulfur, such as $Na_2SO_3H_3^+$, $NaKSO_3H_3^+$ and $Na_3SO_4^+$, indicate the formation of sodium and potassium sulfates during the electroless copper plating process, with the sulfate group coming from the copper salt ($CuSO_4•5H_2O$). The presence of these species on the surface resulted in rather weak Cu^+ signals (not shown).

The negative secondary ion mass spectra in the range of m/z 11–90 are plotted in figure 8, showing the detection of ions of CH^-, O^-, OH^-, C_2H^-, CN^-, CNO^- and CO_2H^-. It is worth noting that in comparison with the control and $AgNO_3$-activeted PI films (figure 3), the abundance of C_3N^- (the peak at m/z 50) on the electroless plated copper samples decreased significantly, suggesting that their sources are different from each other. Specifically, the intensity ratio C_3N^-/CN^- for the $AgNO_3$-activeted samples and electroless plated copper samples is approximately 0.3 and 0.1, respectively. It has been reported that intensity ratios of appropriate species are useful in differentiating chemical structures of aliphatic hydrocarbon polymers [49–51] and gauging cross-linking degrees of polydimethylsiloxane [52], ethyl lactate [53] and poly(methyl methacrylate) [54]. By noticing that Na_2-EDTA was used as a chelate in the electroless plating process, it is inferred that the nitrogen-containing species detected on the plated copper surfaces originated from Na_2-EDTA. The ion CO_2H^- detected on the electroless plated copper surface is likely due to residues of formic acid (HCOOH) resulted from the oxidation of the reducing agent formaldehyde in the electroless plating process. The relatively weak SO_2^- and SO_3^- ions are due to sulfates left on the surface, from the copper sulfate used as the copper source in the electroless plating bath.

Although the surface of the electroless-plated copper layer shows a plenty of contaminants originated from the plating bath, figure 8 does show the detection of Cu^-, CuO^- and $CuOH_2^-$, revealing the presence of a native copper oxide layer. The negative secondary ion mass spectra in the range of m/z 90–200 are shown in figure 9, from which several higher mass copper oxide cluster ions are detected. The five peaks from m/

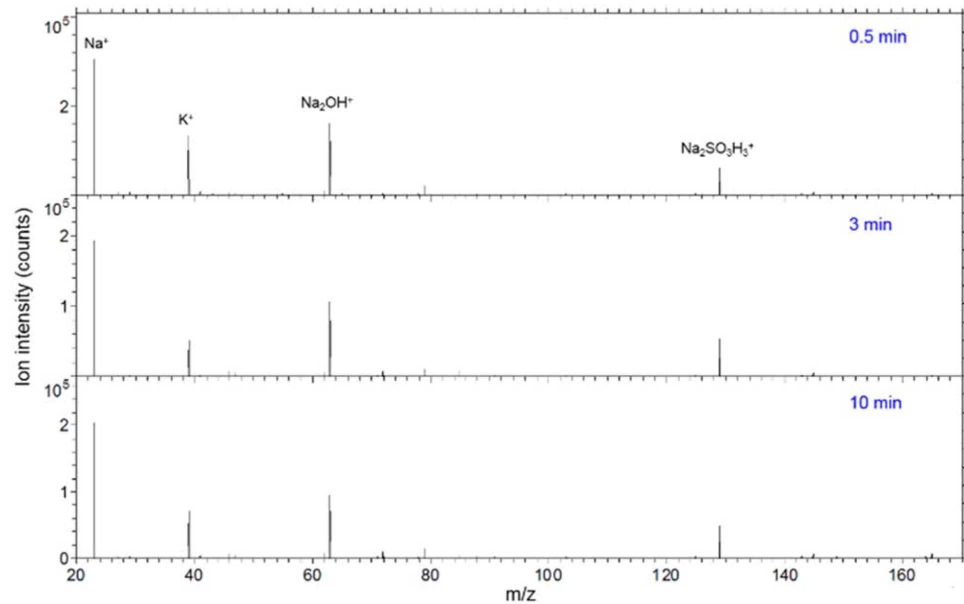

Figure 6. Positive secondary ion mass spectra (m/z 20–170) of copper layers electroless-plated for 0.5, 3 and 10 min on a PI film activated by $AgNO_3$ for 1 min.

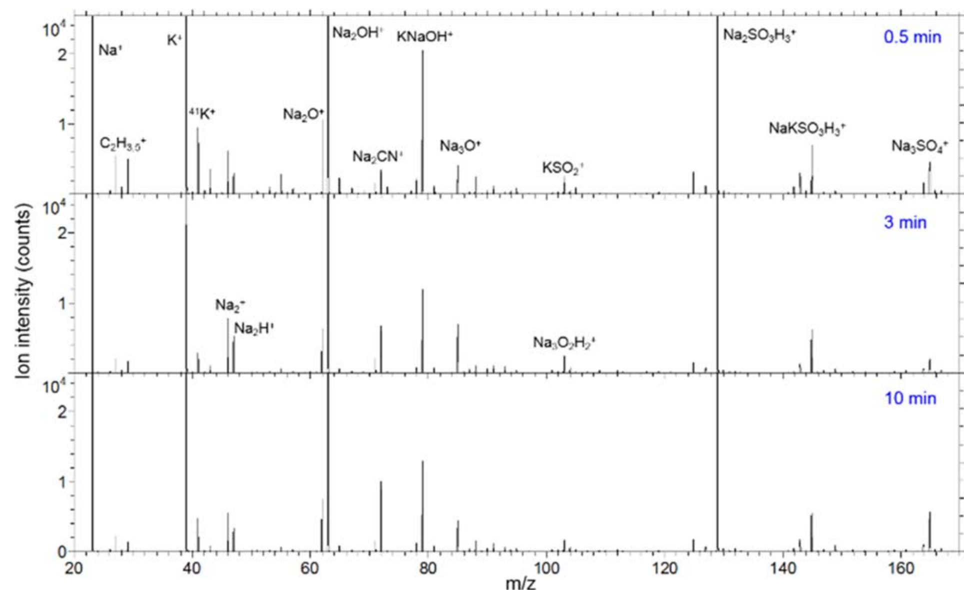

Figure 7. Positive secondary ion mass spectra (m/z 20–170) of copper layers electroless-plated for 0.5, 3 and 10 min on a PI film activated by $AgNO_3$ for 1 min, with the ion intensity scales adjusted to show the less abundant ions.

z 95 to 99 are a combination of CuO_2^-, CuO_2H^- and $CuO_2H_2^-$, with appropriate intensity ratios, which can be readily determined using the isotope cluster calculator of the TOF-SIMS software. Similarly, the four peaks at m/z 105 to 108 are a combination of CuC_2HO^-, $CuCNO^-$ and $CuCNOH^-$. The peaks from m/z 174 to 181 are a combination of $Cu_2O_3^-$, $Cu_2O_3H^-$, $Cu_2O_3H_2^-$ and $Cu_2O_3H_3^-$. Also identified are $Cu(CN)_2^-$, $Cu_2O_2^-$ and $Cu_2O_2H^-$.

As shown in the TOF-SIMS results described above, the surface chemistry of the electroless-plated copper is complicated in that each chemical used in the plating bath left residues on the surface. This is readily explained by the fact that the plating process is a wet chemistry one involving various chemicals. On the other hand, because TOF-SIMS is extremely surface sensitive, probing the outermost 1–3 nm of a sample, the species detected by TOF-SIMS should be only in that depth range. This is supported by the fact that the copper native oxide was also detected. The electroless-plated copper film was depth profiled for estimating the thickness of those surface species on and the copper native oxide of it. Because copper films plated for 3 min and less were too thin to serve as a metallic film as confirmed by conductivity measurement [34], only the depth profiles for the 10-min electroless-

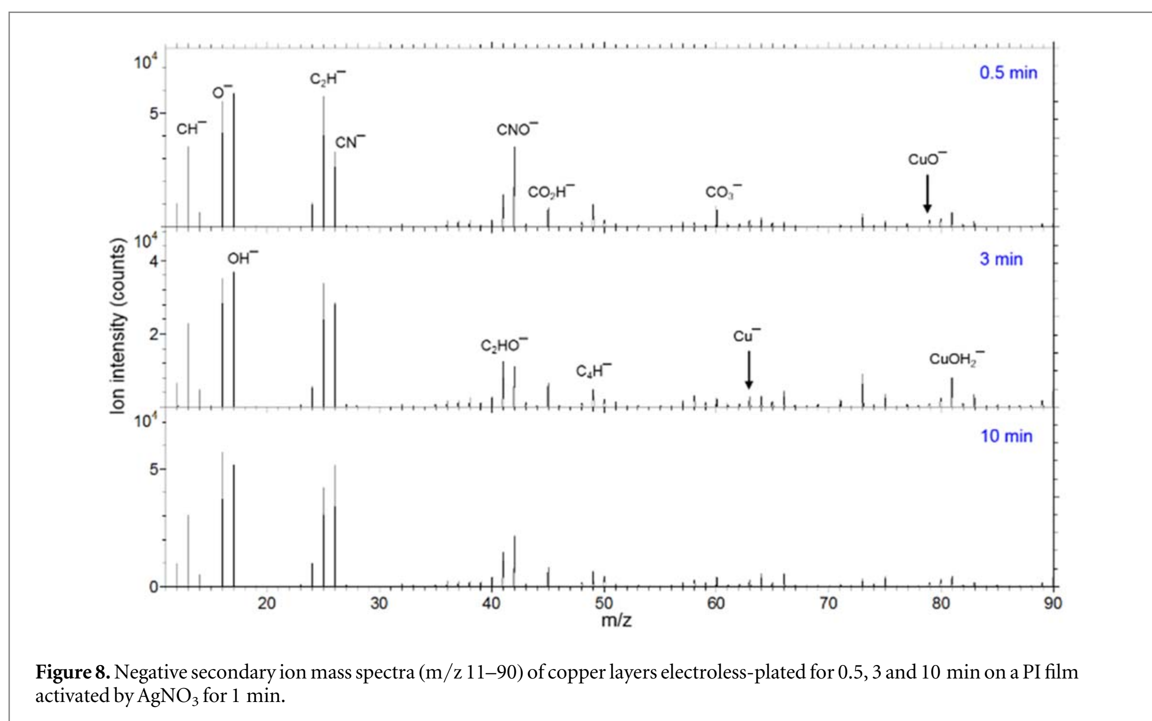

Figure 8. Negative secondary ion mass spectra (m/z 11–90) of copper layers electroless-plated for 0.5, 3 and 10 min on a PI film activated by $AgNO_3$ for 1 min.

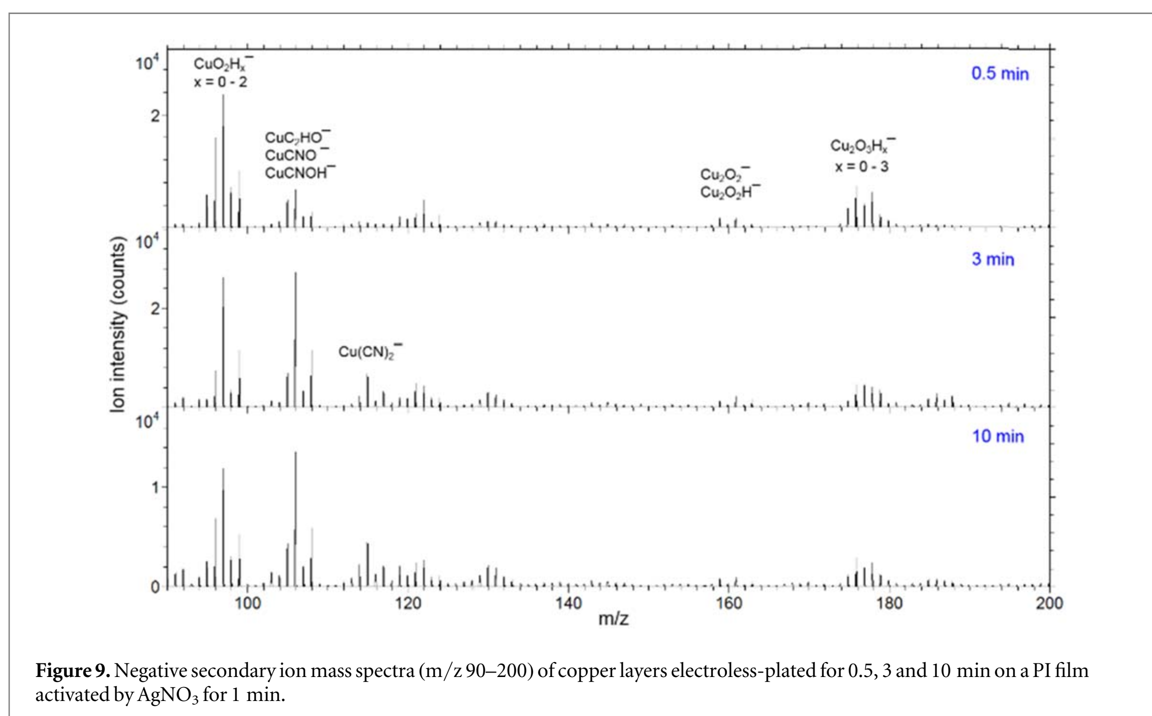

Figure 9. Negative secondary ion mass spectra (m/z 90–200) of copper layers electroless-plated for 0.5, 3 and 10 min on a PI film activated by $AgNO_3$ for 1 min.

plated copper sample are shown in figure 10 to investigate as how the surface species, including the native copper oxide, change as a function of depth.

Shown in figure 10(a) are shallow depth profiles of copper oxide species. Also shown is a cluster copper species Cu_3^- at m/z 191 (i.e. $^{63}Cu_2^{65}Cu^-$), which is used to represent metallic copper because its ion yield is much greater in metallic copper than in a copper oxide. This cluster ion is not detected on the surface (figure 9), but its intensity increases rapidly within the first 6–8 nm and gradually plateaus thereafter (figure 10(a)). The copper oxide related species CuO^-, CuO_2^-, $Cu_2O_2^-$ and $Cu_2O_3H_2^-$ shown in figure 10(a) have a peak at 2.2, 1.8, 2.2 and 1.6 nm, respectively. Therefore, our TOF-SIMS depth profiling results confirmed that the first 6 nm or so of the electroless plated copper layer is characterized as the native copper oxide region, after which it becomes metallic.

Figure 10(b) shows depth profiles of species Na^-, CN^-, CNO^-, CHO_2^-, C_3N^- and SO_3^-, which, as discussed before, are considered surface contamination associated with the chemicals used in the electroless plating bath. Species Na^-, CN^- and SO_3^- show their peaks at 1.0 nm, while CNO^-, CHO_2^- and C_3N^- at 0.6 nm. It is interesting to note that CHO_2^-, which represents carboxylate originating from formic acid as

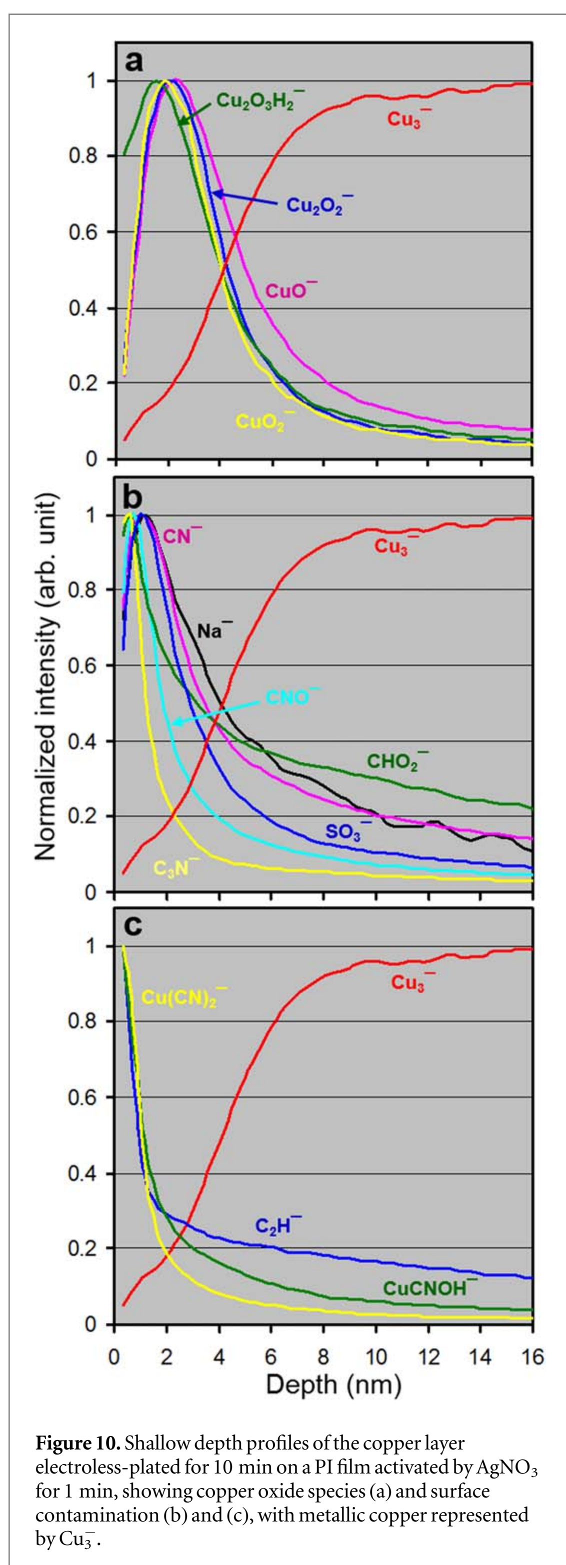

Figure 10. Shallow depth profiles of the copper layer electroless-plated for 10 min on a PI film activated by $AgNO_3$ for 1 min, showing copper oxide species (a) and surface contamination (b) and (c), with metallic copper represented by Cu_3^-.

a result of oxidation of the reducing agent formaldehyde, has a larger tail into the copper film, in comparison with the other species. This indicates the possibility that the reducing agent is a source of the impurities of an electroless-plated copper film. However, because TOF-SIMS is not a quantitative technique [55–57] without the use of a standard, it is not possible to quantitatively estimate the level of the contaminants. Nevertheless, the depth profiles shown in figure 10(b) shows the changes of contaminants in the first 10 nm or so.

Figure 10(c) shows the depth profiles of C_2H^-, CuCNOH$^-$ and $Cu(CN)_2^-$, in which C_2H^- is most likely due to adventitious hydrocarbon and the other two copper-containing species may be a reflection of the presence of copper cyanide. In contrast to copper oxide species in figure 10(a) and other surface species in figure 10(b), the three species shown in figure 10(c) have no peaks and whose intensities decrease rapidly within the first 2 nm, confirming that they are present on the very surface.

Finally, shown in figure 11 is the surface morphology of the 10-min electroless plated copper film, which has an Rq of 48 nm mainly due to the larger particles that are as high as 600 nm. Without counting these larger particles, the smoother areas have a much smaller Rq of 14 nm. In comparison with the 1-min $AgNO_3$-treated PI surface, which is quite smooth with an Rq of 6 nm (figure 5(b)), the electroless plated copper surface is much rougher. Nevertheless, the roughness of our electroless-plated copper is quite reasonable in comparison with reported results [30, 33]. One possibility for the observed large particles is that they are caused by precipitations formed in the solution falling on the substrate and merging with the plated metal film. If this is true, then positioning the substrate vertically in the plating solution will minimize the formation of the large particles. In addition, depth profiling such particles using TOF-SIMS ought to be able to help clarify this hypothesis, which is a future work important to understanding the large particles.

4. Conclusions

TOF-SIMS and AFM were used to follow the surface chemistry of electroless-plated copper on an silver nitrate activated a PI film, using a plating bath containing a copper source (copper sulfate pentahydrate), two chelates (disodium ethylenediaminetetraacetate and potassium sodium tartrate tetrahydrate) and a reducing agent (formaldehyde). As revealed by AFM, the immersion time for the PI film in the silver nitrate solution impacted the roughness of the surface.

While the 1-min immersion resulted in a smooth and fully silver-activated surface, the 20-min immersion induced aggregates. Therefore, one should use a brief immersion to make a smooth silver activated surface for PI films. The TOF-SIMS investigation on the electroless-plated copper samples confirmed: (a) the presence of copper oxide and (b) surface contamination associated with the chemicals used in the plating bath on the copper samples. Shallow TOF-SIMS depth profiling on a 10-min plated copper sample shows that the copper oxide species (CuO^-, CuO_2^-, $Cu_2O_2^-$ and $Cu_2O_3H^-$) span over 6 nm and peak at 1.6–2.2 nm, while contaminant species peak at 1.0 nm (Na^-, CN^-

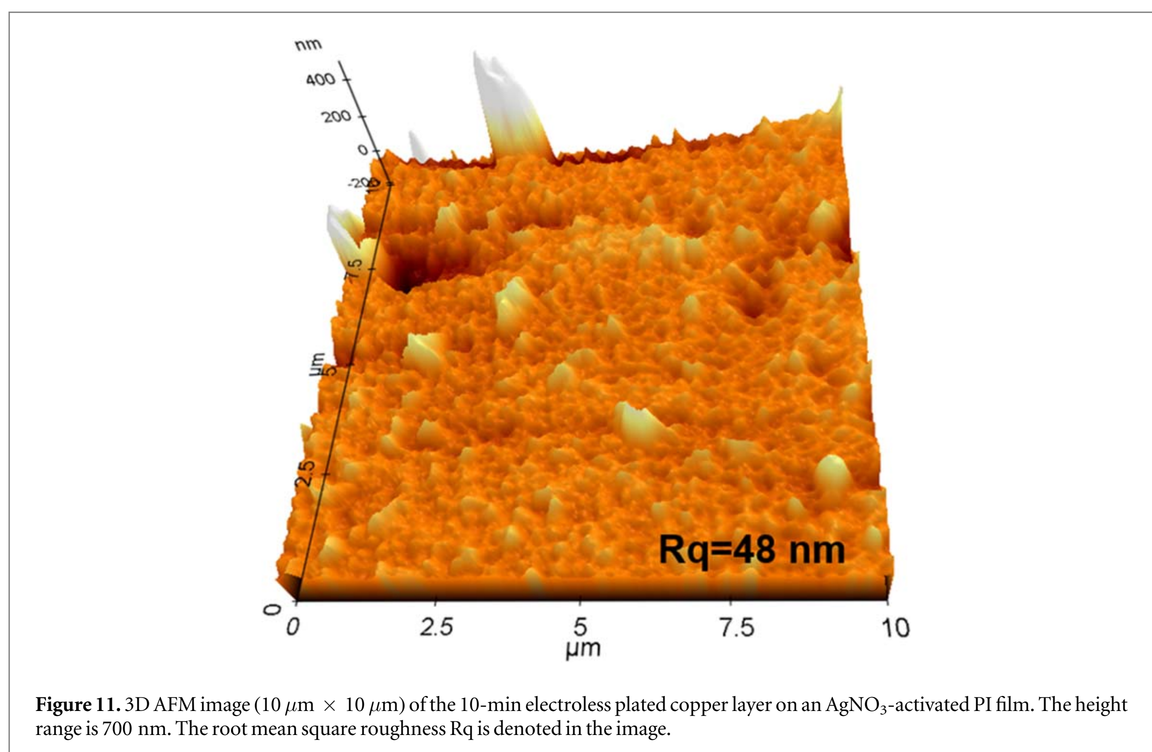

Figure 11. 3D AFM image (10 μm × 10 μm) of the 10-min electroless plated copper layer on an $AgNO_3$-activated PI film. The height range is 700 nm. The root mean square roughness Rq is denoted in the image.

and SO_3^-) or 0.6 nm (CNO^-, CHO_2^- and C_3N^-). By contrast, the intensities of contaminant species C_2H^- and $Cu(CN)_2^-$, without having a peak, decrease rapidly within the first 2 nm. All species mentioned above are limited to the first 6 nm, except for CHO_2^-, an ion characteristic for carboxylates, that shows a larger tail penetrating into the copper layer. The source of this ion is believed to be from formic acid, which is resulted from the reducing agent formaldehyde used in the electroless plating bath. This may be a contributor to the impurity of an electroless-plated copper layer. The surface contamination, revealed by TOF-SIMS, on the electroless-plated copper layer will deviate its surface chemistry from that of normal copper (e.g., that of a sputter-deposited copper film). This should be kept in mind when a surface modification is to be carried out on an electroless-plated copper layer.

Acknowledgments

The authors gratefully acknowledge the financial support by the National Natural Science Foundation of China (Grant No. 51875253), the 111 Project (Grant No. B18027), and the Fundamental Research Funds for the Central Universities (Grant No. JUSRP21910).

ORCID iDs

Yu Liu https://orcid.org/0000-0002-7945-7462

References

[1] Wong W S and Salleo A 2009 *Flexible Electronics: Materials and Applications* (United States: Springer Science & Business Media)
[2] Subramanian V and Lee T 2012 *Nanotechnology* **23** 340201
[3] Lind J U, Busbee T A, Valentine A D, Pasqualini F S, Yuan H, Yadid M, Park S-J, Kotikian A, Nesmith A P and Campbell P H 2017 *Nat. Mater.* **16** 303–8
[4] Xie Z, Avila R, Huang Y and Rogers J A 2020 *Adv. Mater.* **32** 1902767
[5] Wang Z, Cong Y and Fu J 2020 *J. Mater. Chem.* B **8** 3437–59
[6] Wei C, Qin H, Chiu C-P, Lee Y-S and Dong J 2015 *J. Manuf. Syst.* **37** 505–10
[7] Zhou N, Liu C, Lewis J A and Ham D 2017 *Adv. Mater.* **29** 1605198
[8] Tricot F, Venet C, Beneventi D, Curtil D, Chaussy D, Vuong T P, Broquin J E and Reverdy-Bruas N 2018 *RSC Advances* **8** 26036–46
[9] Jin S W, Lee Y H, Yeom K M, Yun J, Park H, Jeong Y R, Hong S Y, Lee G, Oh S Y and Lee J H 2018 *ACS Appl. Mater. Interfaces* **10** 30706–15
[10] Ishikawa A, Kato T, Takeyasu N, Fujimori K and Tsuruta K 2017 *Appl. Phys. Lett.* **111** 183102
[11] Singh M, Haverinen H M, Dhagat P and Jabbour G E 2010 *Adv. Mater.* **22** 673–85
[12] Shen W, Zhang X, Huang Q, Xu Q and Song W 2014 *Nanoscale* **6** 1622–8
[13] Vaithilingam J, Simonelli M, Saleh E, Senin N, Wildman R D, Hague R J, Leach R K and Tuck C J 2017 *ACS Appl. Mater. Interfaces* **9** 6560–70
[14] Kvítek L, Panáček A, Soukupova J, Kolář M, Večeřová R, Prucek R, Holecova M and Zbořil R 2008 *J. Phys. Chem.* C **112** 5825–34
[15] Raut N C and Al-Shamery K 2018 *J. Mater. Chem.* C **6** 1618–41
[16] Bourassa J, Ramm A, Feng J Q and Renn M J 2019 *SN Appl. Sci.* **1** 517
[17] Kang C W, Choi J, Ko J H, Kim S-K, Ko Y-J, Lee S M, Kim H J, Kim J P and Son S U 2017 *J. Mater. Chem.* A **5** 5696–700
[18] Gokhale P, Mitra D, Sowade E, Mitra K Y, Gomes H L, Ramon E, Al-Hamry A, Kanoun O and Baumann R R 2017 *Nanotechnology* **28** 495301
[19] Walker S B and Lewis J A 2012 *J. Am. Chem. Soc.* **134** 1419–21

[20] Khaleel H R, Al-Rizzo H M, Rucker D G and Mohan S 2012 *IEEE Antennas Wirel. Propag. Lett.* **11** 564–7
[21] Spechler J A, Koh T W, Herb J T, Rand B P and Arnold C B 2015 *Adv. Funct. Mater.* **25** 7428–34
[22] Fang Y, Hester J G, deGlee B M, Tuan C-C, Brooke P D, Le T, Wong C-P, Tentzeris M M and Sandhage K H 2016 *J. Mater. Chem.* C **4** 7052–60
[23] Mahajan A, Hyun W J, Walker S B, Lewis J A, Francis L F and Frisbie C D 2015 *ACS Appl. Mater. Interfaces* **7** 1841–7
[24] Bindra P and White J R 1990 *Electroless Plating: Fundamentals and Applications* (Norwich, NY: Noyes Publications/William Andrew Publishing)
[25] Deckert C A 1995 *Plating & Surface Finishing* **82** 48–55
[26] Sharma A, Cheon C-S and Jung J P 2016 *J. Microelectron. Pack. Soc.* **23** 1–6
[27] Shacham-Diamand Y, Sverdlov Y, Friedberg S and Yaverboim A 2017 *Nanomaterials for 2D and 3D Printing* ed S Magdassi and A Kamyshny (Weinherim, Germany: Wiley-VCH Verlag GmbH & Co. KGaA)
[28] Cai J, Zhang M, Sun Z, Zhang C, Liang C, Khan A, Ning X, Ge H, Feng S-P and Li W-D 2019 *J. Mater. Chem.* C **7** 4363–73
[29] Dow W-P, Liao G-L, Huang S-E and Chen S-W 2010 *J. Mater. Chem.* **20** 3600–9
[30] Lin Y-M and Yen S-C 2001 *Appl. Surf. Sci.* **178** 116–26
[31] Park S-J, Lee E-J and Kwon S-H 2007 *Bull. Korean Chem. Soc.* **28** 188–92
[32] Hanna F, Hamid Z A and Aal A A 2003 *Mater. Lett.* **58** 104–9
[33] Ji E S, Cha H G, Kim C W and Kang Y S 2008 *Mol. Cryst. Liq. Cryst.* **492** 275/[639]-282/[646]
[34] Cai W-R, Chen Y-Q, Liu Y, Yan H, Zhang J, Jin X, Zhang Y-Z, Deng Y-Q and Lau W-M 2017 *IEEE Trans. Comp. Pack. Manuf. Technol.* **7** 1552–9
[35] Korolkov I V, Borgekov D B, Mashentseva A A, Guven O, Atıcı A L, Kozlovskiy A L and Zdorovets M V 2017 *Chem. Pap.* **71** 2353–8
[36] Muench F, Eils A, Toimil-Molares M E, Hossain U H, Radetinac A, Stegmann C, Kunz U, Lauterbach S, Kleebe H-J and Ensinger W 2014 *Surf. Coat. Technol.* **242** 100–8
[37] Jang G G, Hawkridge M E and Roper D K 2012 *J. Mater. Chem.* **22** 21942–53
[38] Benninghoven A 1994 *Angew. Chem. Int. Ed.* **33** 1023–43
[39] Vickerman J C and Winograd N 2015 *Int. J. Mass Spectrom.* **377** 568–79
[40] Belu A M, Davies M C, Newton J M and Patel N 2000 *Anal. Chem.* **72** 5625–38
[41] Nie H-Y 2010 *Anal. Chem.* **82** 3371–6
[42] Mahoney C M 2010 *Mass Spectrom. Rev.* **29** 247–93
[43] Thiel V and Sjövall P 2011 *Ann. Rev. Earth Planet. Sci.* **39** 125–56
[44] Fletcher J S, Lockyer N P, Vaidyanathan S and Vickerman J C 2007 *Anal. Chem.* **79** 2199–206
[45] Shard A, Brewer P, Green F and Gilmore I 2007 *Surf. Interface Anal.* **39** 294–8
[46] Zheng L, Wucher A and Winograd N 2008 *Anal. Chem.* **80** 7363–71
[47] Tardio S and Abel M-L 2015 *J. Vac. Sci. Technol.* A **33** 05E122
[48] Jones E A, Lockyer N P, Kordys J and Vickerman J C 2007 *J. Am. Soc. Mass. Spectrom.* **18** 1559–67
[49] Nie H-Y 2016 *J. Vac. Sci. Technol.* B **34** 030603
[50] Briggs D 1990 *Surf. Interface Anal.* **15** 734–8
[51] Nie H-Y 2017 *Surf. Interface Anal.* **49** 1431–41
[52] Bao C *et al* 2015 *ACS Appl. Mater. Interfaces* **7** 8515–24
[53] Ligot S, Bousser E, Cossement D, Klemberg-Sapieha J, Viville P, Dubois P and Snyders R 2015 *Plasma Process. Polym.* **12** 508–18
[54] Naderi-Gohar S, Huang K M, Wu Y, Lau W M and Nie H-Y 2017 *Rapid Commun. Mass Spectrom.* **31** 381–8
[55] Sodhi R N S 2004 *Analyst* **129** 483–7
[56] Walker A V 2008 *Anal. Chem.* **80** 8865–70
[57] Shard A G, Spencer S J, Smith S A, Havelund R and Gilmore I S 2015 *Int. J. Mass Spectrom.* **377** 599–609